Reflection of water waves in a channel with corrugated bed

By T. BROOKE BENJAMIN

Mathematical Institute, 24/29 St Giles, Oxford OX1 3LB, UK

B. BOCZAR-KARAKIEWICZ

I.N.R.S.-Océanologie, Université du Québec, Rimouski, Québec G5L 3A1, Canada

AND W. G. PRITCHARD

Department of Mathematics, Pennsylvania State University, University Park, PA 16802, USA

Intended as a contribution towards understanding the multiple processes entailed in the development of coastal sand bars due to wave action, this theoretical and experimental study deals with the Bragg reflection of long-crested surface waves in a water channel whose bed is corrugated sinusoidally. The present findings complement and in a few respects improve upon those in previous investigations, particularly Davies & Heathershaw (1984).

In §2 a linearized theory is presented, being directed to the elucidation of experimental situations where monochromatic waves propagate into a channel with a limited stretch of corrugations on its bed and an imperfectly absorbing beach at its far end. Allowance is made fully for dispersive effects (§2.2) and approximately for small frictional effects (§2.3). Points of interpretation (§2.4) include accounts of degenerate but non-trivial solutions that apply at frequencies terminating the *stopping band*, wherein the spatial wavefield has an exponential envelope. The experimental results presented in §4 derive from measurements of the wavefield over a stretch of 24 corrugations, at various frequencies both inside and outside the stopping band. Quantitative comparisons (§§4.2 and 4.3) demonstrate close agreements with the theory.

1. Introduction

This paper reports one stage of a long-continuing investigation into properties of the more or less parallel sand bars that can form on gently sloping beaches, as in the Baltic Sea, in the Great Lakes and off the South-East coast of England (e.g. see Saylor & Hands 1970; Lau & Travis 1973; Short 1975). The present theoretical and experimental contribution deals with a simpler hydrodynamic problem highly relevant to the explanation of sand bars. The account focuses, in certain respects more sharply than accomplished hitherto, on the process whereby surface waves can be reflected by fixed sinusoidal corrugations on the bed of a water channel.

Our interest in the subject of sand-bar formation was stimulated during a visit by B.B.-K. to the Fluid Mechanics Research Institute at the University of Essex in 1974, when the experiments reported here were begun. In the course of previous experiments on wave absorption by erodible beaches, she had noticed that bars typically developed with spacings about half the local wavelength of the incident
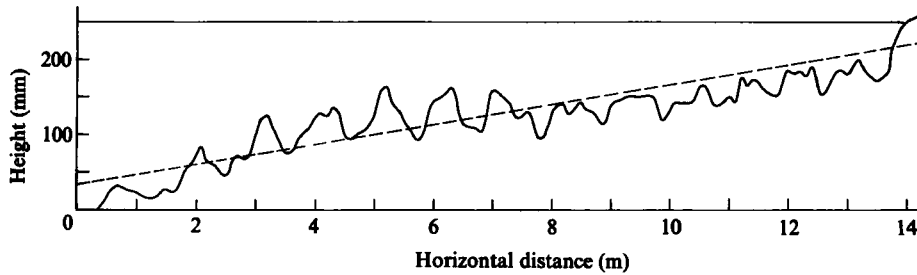
FIGURE 1. The profile of a sand beach after 78900 periods ($\approx$ 39 h) of wave action over it. ----
indicates the initial profile of the beach, which had a slope of 1:75. The waves were initiated in a
uniform channel of depth 0.25 m, having period 1.78 s and wavelength 2.50 m. The amplitude of
the incident wavelength was approximately 30 mm.

wavetrain. An example of this phenomenon is given in figure 1, which shows the
profile of an originally plane beach of sand after 78900 cycles of wave action. The
gradual development of this profile was a complex process in several stages, to which
further reference will be made in §5. The final effect in question is evident in the
figure, however, namely the presence of bars spaced at distances roughly half the
wavelength, 2.5 m, of the incident surface waves. Such observations pointed to the
possibility of the bars being caused by a standing-wave component of the wavefield,
for it is well known that the action of (time-periodic) standing waves on an erodible
bed can generate undulations in the bed at half the wavelength of the water
waves.

The process in question is demonstrated more clearly in figure 2, which exhibits
successive phases in the development of undulations in a sand bed under the action
of small-amplitude waves that had a distinct standing-wave component due to
partial reflection from a rigid beach. This process is slow and quite complicated: for
example, the ripples of comparatively short wavelength evident in figure 2 appear to
play a pivotal role in the formation of the longer undulations. Nevertheless, although
details of the process escape precise analysis, its eventual outcome is plain enough for
a secure association of cause and long-term effect.

The possibility of an interactive, gradually cumulative mechanism of sand-bar
formation is thus suggested. Initial corrugations on an erodible bed with wavelength
about half that of incident surface waves will, exemplifying the phenomenon of
Bragg reflection, generate a standing-wave component of the liquid motion whose
action will promote the growth of the corrugations. In turn, enlargement of the
corrugations will reinforce the standing-wave component. Note that Bragg reflection
occurs over a range of temporal frequencies, the *stopping band*, wherein the
wavelengths of waves in a corresponding uniform channel would be nearly twice that
of the corrugations, and spatial phase-locking over the corrugations is a concomitant
of the reflection mechanism. Although precise tuning of the water-wave frequency to
the centre of the stopping band optimizes reflection, the mechanism in question
remains operative throughout the stopping band.

The subject of Bragg reflection, a name inherited from its origins in crystal-
lography, has been explored in a wide range of physical contexts. For basic ideas and
details of various applications, reference can be made to the famous monograph
by Brillouin (1953) or the extensive review article by Elachi (1976). Oceanographic
applications have been considered by Rhines (1970), Davies & Heathershaw (1984),
Mitra & Greenberg (1984), Mei (1985), Kirby (1986a, b) and many others, among
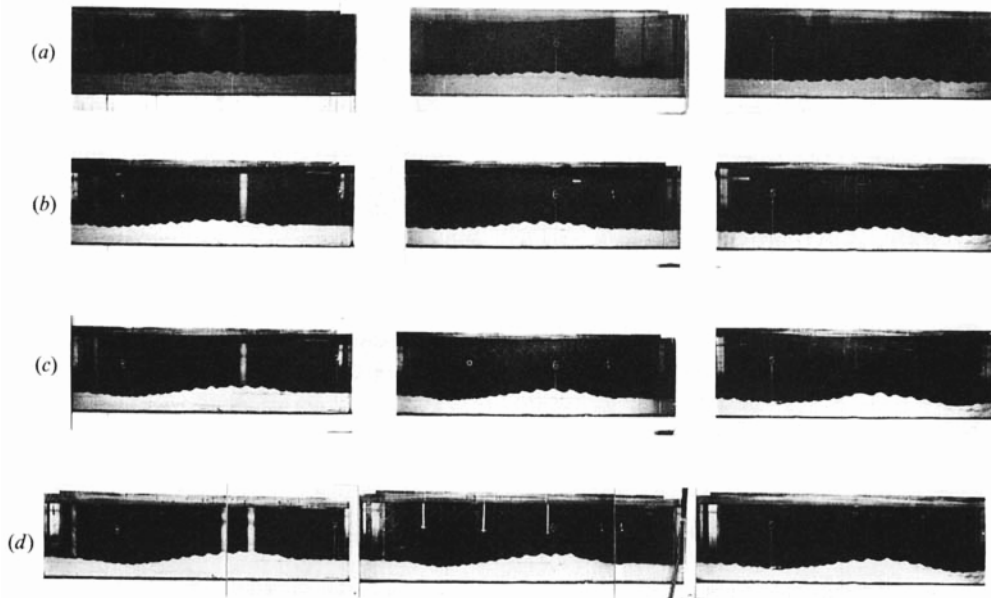
FIGURE 2. Photographs of the sand bed of a channel showing the development of undulations through wave action. The mean water depth was 0.252 m and the period T of the waves was 2.10 s, corresponding to a wavelength of 3.20 m. The bed was flat at time $t = 0$. (a) $t/T = 2.99 \times 10^4$ ($t = 17.4$ h); (b) 1.03×10^5 (59.9 h); (c) 1.83×10^5 (106.6 h); (d) 2.61×10^5 (152.0 h). The markings indicate distance in m from the wavemaker.

which antecedents the paper by Davies & Heathershaw is closest in substance to the present contribution. They reported some experimental observations on long waves propagated across a patch with bottom corrugations in a wave tank. Their main results were measurements of a reflection coefficient for the corrugated patch, as a function of wave frequency, and measurements of the magnitude of the reflected-wave component as a function of position along the channel. The most striking confirmation by these results was that the rippled patch can indeed act as a strong reflecting barrier at frequencies near the so-called *resonance* frequency, that is, near the centre of the stopping band. A quite good general description of Davies & Heathershaw's experimental data is provided by their own partial theory and by the ray-tracing theories of Mei (1985) and Kirby (1986*a*).

Several marginally doubtful aspects attended these previous empirical observations, however, suggesting that a closely detailed agreement with the data should not be expected even though the broad outline of them is more or less well captured by the theories. In the first place, the wavefield seems to have had a fairly high harmonic content, which suggests that nonlinear effects were hardly negligible. Specifically, the amplitude of the first harmonic appears to have been at least 20 % of the fundamental amplitude, in some cases as much as 40 %. Although allowance for weak nonlinear effects can be readily enough incorporated into theoretical models (e.g. as done by Kirby 1986*b*), attendant difficulties are nevertheless posed in practice when empirical methods are used to estimate and interpret quantities such as amplitude and phase angle for supposedly monochromatic waveforms. The methods used by Davies & Heathershaw to determine the magnitude of the reflected-wave component are also open to question. The procedure in fact followed is not fully

defined in their paper, and it must be regarded sceptically because the magnitude of the reflected wave, relative to that of the transmitted wave, was recorded as having considerable variation over stretches of the channel where the bottom was flat. A further cause for doubt is that, in some of the experiments recorded, the absorption properties of the beach terminating their channel appeared to vary markedly with small changes in frequency (e.g. see their figure 6*b*), which behaviour is not normally associable with fixed plane beaches.

The present theoretical and experimental study is complementary to those cited above, but special emphasis is given to several points of interpretation highlighted by empirical observations. Although the theory presented in §2 is less general than those developed by Mei (1985) and Kirby (1986*a*, *b*), it has the advantages of being comparatively straightforward and being directed primarily towards the explanation of experimental results. A notable feature of our calculations is the allowance for an arbitrary level of the backward-travelling wave component reflected from a beach at the far end of the channel. Attention is also given to the effects of viscous damping, and to the degenerate but non-trivial solutions that hold for frequencies at the ends of the stopping band.

Our experimental channel had a wavemaker near one end, a rigid plane beach at the other end, and an intervening section in which the bed was sinusoidally corrugated for 24 wavelengths (see §3). The main experimental findings were derived from careful measurements of surface-wave amplitude as a function of position along the channel, at each of several accurately controlled frequencies of the wavemaker. These frequencies were disposed both inside and outside the stopping band, and respective to each range of frequencies a variety of behaviour predicted theoretically was found to be confirmed with good accuracy by the experimental results (see §§4.2, 4.3). It is notable that in these experiments the water-wave amplitudes were always very small, typically less than 0.1 mm in comparison with a mean water depth of 30 mm. Since maximum wave slopes were thus less than $2\pi \times 0.1/30 = 0.021$, the waveforms had negligible harmonic content. The scale of the experiments was such that some corrections for dissipative effects were needed in order to interpret the results satisfactorily by means of perfect-fluid theory. It appeared, however, that these effects played only a minor role in the principal phenomena observed.

2. Theory

The problem to be treated take its simplest form when a long-wave approximation is adopted, and this model will be examined first. A correct but very abbreviated account of it was included by Rhines (1970) in reviewing various oceanographic applications of ideas about wave propagation in periodic media. Being comparatively easy to understand, the results found on this basis will serve as a guide for the more accurate theoretical model that will be used for comparisons with the experiments.

2.1. *The long-wave approximation*

Suppose that in a straight channel of uniform span, the depth $h(x)$ of water at rest is a gradually varying function of horizontal distance x. For infinitesimal waves of great length in the water, the elevation $\zeta(x,t)$ of the free surface above its undisturbed level satisfies

$$\zeta_{tt} = g(h\zeta_x)_x, \qquad (1)$$

which equation is obtained according to the standard approximations of shallow-

water theory (cf. Stoker 1957, §2.2). In the present application the bottom of the channel is taken to be deformed by small-amplitude corrugations with wavelength $\frac{1}{2}\lambda = \pi/k$. Thus, writing $z = kx = 2\pi x/\lambda$ and letting H denote the mean depth of water, we have

$$h = H(1 + \delta \cos 2z) \quad \text{with } |\delta| \ll 1.$$

We further assume the wave motion to be simple-harmonic in time, writing $\zeta = \hat{\zeta}(z)$ $\sin(\omega t + \theta)$ where θ is a disposable real phase constant. (Note that values of θ differing by $\frac{1}{2}\pi$ can be assigned to two independent solutions in order to compose a complete description of the wavefield.) In this case (1) becomes

$$\frac{\mathrm{d}}{\mathrm{d}z}\left\{(1 + \delta \cos 2z)\frac{\mathrm{d}\hat{\zeta}}{\mathrm{d}z}\right\} + \gamma^2 \hat{\zeta} = 0 \qquad \text{with} \quad \gamma = \frac{\omega}{\omega_0}, \tag{2}$$

where $\omega_0 = k(gH)^{\frac{1}{2}}$ is the frequency of waves that have wavelength $\lambda = 2\pi/k$ propagating in water of *uniform* depth H. As may be expected, the most prominent effects of the corrugations will be found to arise when $\gamma = 1$. Without significant loss of generality, we shall henceforth take δ to be positive.

The substitution $\hat{\zeta} = (1 + \delta \cos 2z)^{-\frac{1}{2}}Z(z)$ reduces (2) to normal form, which may be further reduced to Mathieu's equation by the neglect of terms that are relatively $O(\delta^2)$. Available results concerning Mathieu's equations could therefore be applied. To the order of approximation that will suffice at present in powers of δ, however, it is equally simple to derive the needed results directly from (2), and this approach is helpful as a precedent for the more accurate, dispersive-wave theory to be developed in §2.2.

According to Floquet's theorem about differential equations with periodic coefficients, the two independent solutions of (2) have the form $\mathrm{e}^{\pm\mu z} \times$ (periodic function of $\pm z$). The square of this exponent is a real analytic function of the two parameters δ and γ^2 in (2), and the nature of the solutions, particularly respecting their physical interpretations, changes accordingly as $\mu^2 > 0$ or $\mu^2 < 0$. In the first case, the solution having the factor $\mathrm{e}^{-\mu z}$ with $\mu > 0$ describes a train of standing waves that attenuates in the z-direction and transmits no energy. The attenuation is not, of course, a dissipative effect. Rather, the channel presents a purely reactive impedance to excitation at the respective frequency, like a transmission line excited at a frequency in a cutoff range. In the case that $\mu^2 < 0$ and so μ is purely imaginary, transmitted waves can be described by a combination of solutions whose dependence on z is quasi-periodic.

We proceed to obtain a first approximation to μ for small δ, but in the first place without restriction on the magnitude of $1 - \gamma^2$. Solutions of (2) are considered in the anticipated form

$$\hat{\zeta} = \mathrm{e}^{\mu z}(A \sin z + B \cos z + \ldots).$$

Terms in $\sin 3z$ and $\cos 3z$ are seen from (2) to be next in the expansion; but having coefficients that are $O(A\delta, B\delta)$ as $\delta \to 0$ these terms can be neglected in the first approximation to μ in powers of δ. Hence, after substitution of this expression for ζ into (2), separation of the terms in $\sin z$ and $\cos z$ gives respectively

$$\left.\begin{array}{l} \{1 - \gamma^2 - \mu^2 + \frac{1}{2}\delta(1 + \mu^2)\}A + 2\mu B = 0, \\[2mm] 2\mu A - \{1 - \gamma^2 - \mu^2 - \frac{1}{2}\delta(1 + \mu^2)\}B = 0, \end{array}\right\} \tag{3}$$

which show that

$$(1-\gamma^2-\mu^2)^2 - \tfrac{1}{4}\delta^2(1+\mu^2)^2 + 4\mu^2 = 0. \tag{4}$$

Note first from (4) that the critical condition $\mu = 0$, for which (2) has a periodic solution, occurs at the two values $\gamma_c > 0$ of the frequency ratio $\gamma = \omega/\omega_0$ such that $(1-\gamma_c^2)^2 = \tfrac{1}{4}\delta^2$. That is,

$$\gamma_c = (1 \pm \tfrac{1}{2}\delta)^{\frac{1}{2}}. \tag{5}$$

We introduce the parameter

$$\beta = \frac{1-\gamma^2}{|1-\gamma_c^2|} = \frac{\omega_0^2-\omega^2}{\tfrac{1}{2}\delta\omega_0^2}, \tag{6}$$

so that the *stopping band* of frequencies, within which $\mu^2 > 0$, corresponds to the interval $(-1, 1)$ of β. When β lies inside this interval, or outside but not far from it, a consistent approximation for small δ according to (4) is

$$\mu = \tfrac{1}{2}[\tfrac{1}{4}\delta^2 - (1-\gamma^2)^2]^{\frac{1}{2}} = \tfrac{1}{4}\delta(1-\beta^2)^{\frac{1}{2}}. \tag{7}$$

When $|1-\gamma^2|$ is not comparable with δ, however, the complete small-δ result (4) needs to be used. This equation is a quadratic in μ^2, whose root recovering (7) in the case of small $|1-\gamma^2|$ is

$$\mu^2 = \frac{\gamma(4-\delta^2+\tfrac{1}{4}\gamma^2\delta^2)^{\frac{1}{2}} - 1 - \gamma^2 + \tfrac{1}{4}\delta^2}{1-\tfrac{1}{4}\delta^2}. \tag{8}$$

Note that with $\delta = 0$ this formula gives $\mu^2 = -(1-\gamma)^2$, which correctly reproduces the known properties of long waves in a uniform channel. Putting, $\mu = i\kappa/k$, we obtain $\gamma = \omega/\omega_0 = (k\pm\kappa)/k$, confirming that the frequency ω is proportional to the wavenumber $k\pm\kappa$ that arises from the present description of ζ.

As in the theory of Mathieu's equation, the Floquet exponent μ for solutions of (2) can be represented exactly as the root of an infinite determinant with parameters γ^2 and δ. Hence, by taking successively more rows of the determinant into consideration, improved approximations in higher powers of δ could be obtained for the function $\mu^2 = \mu^2(\delta, \gamma^2)$. It deserves emphasis that (3) and the deductions therefrom constitute a self-consistent first approximation for small δ, even at the lower end of the stopping band ($\beta \to 1$) where $A/B \to 0$ and at the upper end ($\beta \to -1$) where $B/A \to 0$. Although accurate only to $O(\delta)$, the simple result (7) suffices for present purposes.

2.2. *Approximation for dispersive waves*

Guided by the long-wave approximation but aiming to improve upon it, we now develop a theory of Stokes water waves in a channel with a corrugated bottom. The theory is superficially comparable with those developed by Mei (1985) and by Mitra & Greenberg (1984), the latter of whom considered gradual temporal rather than spatial changes in wavetrains reflected by corrugations. But our approach is essentially different from theirs and is directed towards various careful comparisons with the experimental observations to be presented in §4. Take axes (x, y) such that the undisturbed free surface is described by $y = H$ and the bottom $\mathcal{B}$ by

$$y = \delta H \cos 2kx.$$

(For the time being the contracted notation $z = kx$ is relinquished.) Being supposedly generated from rest by conservative forces, the wave motion has a velocity potential $\phi(x, y, t)$ that satisfies

$$\phi_{xx} + \phi_{yy} = 0 \tag{9}$$

in the fluid-filled domain for all t. The kinematical condition satisfied at the bottom is

$$\frac{\partial \phi}{\partial n} = 0 \quad \text{on } \mathscr{B}, \tag{10}$$

where $\partial/\partial n$ denotes the normal derivative. The linearized kinematical and dynamical conditions at the free surface are respectively

$$\zeta_t = \phi_y, \quad \phi_t + g\zeta = 0 \quad \text{on } y = H,$$

between which the elimination of ζ leads to

$$\omega^2 \hat{\phi} = g\hat{\phi}_y \quad \text{on } y = H \tag{11}$$

in the case that $\phi = \hat{\phi}(x, y) \cos(\omega t + \theta)$.
We introduce the transformation

$$\xi = x - (\delta H \operatorname{cosech} 2kH) \sin 2kx \cosh 2k(H - y),$$
$$\eta = y + (\delta H \operatorname{cosech} 2kH) \cos 2kx \sinh 2k(H - y),$$

noting that $y = H$ is transformed into $\eta = H$ and, to first order in δ, the equation $y = -\delta H \cos 2kx$ describing the bottom is transformed into $\eta = 0$. Since this transformation is conformal (i.e. $\xi_x = \eta_y$, $\xi_y = -\eta_x$), its Jacobian $J = \partial(\xi, \eta)/\partial(x, y)$ is the same as $\xi_x^2 + \xi_y^2$, which at once shows that $J = 1 - (4\delta kH \operatorname{cosech} 2kH) \cos 2k\xi \cosh 2k(H - \eta) + O(\delta^2)$.

Again because the transformation is conformal, (9) implies that

$$\hat{\phi}_{\xi\xi} + \hat{\phi}_{\eta\eta} = 0, \tag{12}$$

and to first order in δ the boundary conditions (10) and (11) become

$$\frac{\partial \hat{\phi}}{\partial \eta} = 0 \quad \text{on } \eta = 0 \tag{13}$$

and

$$\omega^2 \hat{\phi} = g J^{\frac{1}{2}} \hat{\phi}_\eta$$
$$= g(1 - \epsilon \cos 2k\xi) \hat{\phi}_\eta \quad \text{on } \eta = H, \tag{14}$$

with $\epsilon = 2\delta kH \operatorname{cosech} 2kH \leqslant \delta$.

A non-trivial solution of the boundary-value problem (12)–(14) is needed in the form indicated by Floquet's theorem, namely a harmonic function whose ξ-dependence for each $\eta \in [0, H]$ is of the type $e^{\mu k\xi} \times (2\pi\text{-periodic function of } k\xi)$. As a first-order approximation in powers of ϵ, the appropriate solution of (12) satisfying (13) is seen to be

$$\hat{\phi} = e^{\mu k\xi} \{C(\sin k\xi \cosh k\eta \cos \mu k\eta - \cos k\xi \sinh k\eta \sin \mu k\eta)$$
$$+ D(\cos k\xi \cosh k\eta \cos \mu k\eta + \sin k\xi \sinh k\eta \sin \mu k\eta)\}. \tag{15}$$

Estimates by inspection similar to those noted in §2.1 show that the next stage of approximation in powers of ϵ would require additional potentials with factors $\sin 3k\xi$ and $\cos 3k\xi$. However, to the order of accuracy already decided by the adoption of (13) and (14) as approximations, the extra terms would not affect the estimation of μ. For the time being we do not assume $|\mu|$ to be small, so covering cases where the ξ-dependence of solutions is determined mainly by the ordinary dispersive properties of Stokes waves rather than by the influence of the corrugations. Allowance is thus

made for the possibility that μ has large imaginary values, such as would preserve the validity of (15) in the case that ω were much different from the frequency

$$\omega_0 = (gk \tanh kH)^{\frac{1}{2}} \tag{16}$$

of waves with the wavelength $\lambda = 2\pi/k$ in water of uniform depth H.

After substitution of (15) into (14), separation of terms in $\sin k\xi$ and $\cos k\xi$ gives respectively

$$\left.\begin{aligned} \{\gamma^2 T - (T - \mu\tau)(1 + \tfrac{1}{2}\epsilon)\} C + \{\gamma^2 T^2\tau - (\tau + \mu T)(1 + \tfrac{1}{2}\epsilon)\} D &= 0, \\ -\{\gamma^2 T^2\tau - (\tau + \mu T)(1 - \tfrac{1}{2}\epsilon)\} C + \{\gamma^2 T - (T - \mu\tau)(1 - \tfrac{1}{2}\epsilon)\} D &= 0, \end{aligned}\right\} \tag{17}$$

in which

$$T = \tanh kH, \quad \tau = \tan \mu kH$$

and

$$\gamma^2 \left(= \frac{\omega^2}{\omega_0^2}\right) = \frac{\omega^2}{gkT}.$$

Hence, from the requirement that the determinant of (17) be zero, it is found that

$$\left(\mu - \gamma^2 T\tau + \frac{\tau}{T}\right)^2 + \left(1 - \gamma^2 - \frac{\mu\tau}{T}\right)^2 = \frac{\tfrac{1}{4}\epsilon^2(1 + \mu^2)(T^2 + \tau^2)}{T^2}. \tag{18}$$

This relation determining μ implicitly as a function of γ^2 and ϵ is accurate only for $\epsilon \ll 1$, but it entails no restriction on values of $|1 - \gamma^2|$. Several points of interpretation are listed as follows.

(i) Upon the substitution of $\mu = i\kappa/k$ which implies $\tau = i \tanh \kappa H = i\tilde{\tau}$, say, the left-hand side of (18) can be factorized to give

$$\omega_0^{-2}(1 - T^2\tilde{\tau}^2)\{\omega^2 - g(k + \kappa) \tanh (k + \kappa)H\}\{\omega^2 - g(k - \kappa) \tanh (k - \kappa)H\}$$

$$= \tfrac{1}{4}\epsilon^2 \left\{1 - \left(\frac{\kappa}{K}\right)^2\right\} \frac{(T^2 - \tilde{\tau}^2)}{T^2}. \tag{19}$$

Our result thus bears out the expected property that, when $\epsilon = 0$, either κ or $-\kappa$ satisfies

$$\omega^2 = g(k + \kappa) \tanh (k + \kappa) H$$

(i.e. then $k \pm \kappa$ comply with the dispersion relation for Stokes waves in a uniform channel).

(ii) According to (18) the two critical values γ_c of γ that correspond to $\mu = 0$, so marking the ends of the stopping band, are given by

$$\gamma_c = (1 \pm \tfrac{1}{2}\epsilon)^{\frac{1}{2}} > 0, \tag{20}$$

which compares with (5). Since $\epsilon \ll 1$ by assumption, the width of the stopping band is thus reduced in the ratio

$$\frac{\epsilon}{\delta} = 2kH \operatorname{cosech} 2kH = R,$$

say, from its values according to the long-wave theory. [It is noteworthy that $\tfrac{1}{4}\epsilon\omega_0$, approximately the frequency difference between the centre and ends of the stopping band, is the same as the 'cutoff frequency' Ω_0 that has a prominent role in Mei's account (1985, (2.30)).]

(iii) Inside the stopping band, or more generally when $|1 - \gamma^2|$ as well as ϵ is small, (18) shows $|\mu|$ to be comparably small; and we can therefore put $\tau = \mu kH$ in a first

approximation, provided kH is not much larger than 1. Hence the first approximation to μ given by (18) is seen to be

$$\mu = \frac{[\frac{1}{4}\epsilon^2 - (1 - \gamma^2)^2]^{\frac{1}{2}}}{1 + kH\,(T^{-1} - \gamma^2 T)}, \tag{21}$$

and it is consistent with this approximation to put $\gamma^2 = 1$ in the denominator on the right-hand side. Thus, reintroducing the parameter β as defined by (6) but with (20) in place of (5) for γ_c^2, we obtain

$$\mu = \frac{\frac{1}{2}\epsilon(1 - \beta^2)^{\frac{1}{2}}}{1 + R}, \tag{22}$$

which compares with (7). It is noteworthy that the formula (20) agrees exactly with the result (18) concerning the condition $\mu = 0$. In figure 6 later, where experimental measurements are presented, graphs of $\mu = \mu(\gamma^2)$ in the stopping band, continued as graphs of the real function $i\mu(\gamma^2)$ outside it, will be plotted both from (21) and from (18).

(iv) In the long-wave limit $kH \to 0$, we have $R = 1$ and so $\epsilon = \delta$. The previous results (5) and (7) are thus recovered from (20) and (22) in this limit.

(v) As is obviously to be expected, the corrugations have a smaller influence on the Stokes waves treated here than on long waves as treated in §2.1, and their influence disappears for very short waves which are insensitive to the presence of the bottom. For example, the maximum real $\mu > 0$ occurs for $\beta = 0$ according to (22), corresponding $\beta = O(\epsilon^2)$ according to (21), and its value is approximately

$$\frac{\frac{1}{2}\epsilon}{1 + R} \equiv \frac{\frac{1}{2}\delta R}{1 + R}. \tag{23}$$

Thus, owing to effects neglected by the long-wave theory, the maximum attenuation rate is reduced in the ratio $2R/(1 + R)$, which decreases monotonically with $kH > 0$ and vanishes in the limit $kH \to 0$. Roughly speaking, the factor $R < 1$ is accountable to the exponential diminution of the wave motion with depth below the surface. The partially compensating factor $2/(1 + R) > 1$ is accountable to the dispersive properties of Stokes waves and might be expected, being the ratio of the phase velocity ω_0/k to the group velocity $d\omega/dk$ of waves at the frequency ω_0 in a uniform channel.

(vi) In the experiments to be reported, the optimal wavelength λ (twice that of the corrugations) equalled $12.0H$, so that

$$2kH = 1.0472, \quad R = 0.8382, \quad 2R/(1 + R) = 0.9120.$$

Correspondingly, the optimal frequency ω_0 given by (16) was lower in the ratio $[(\tanh kH/kH)]^{\frac{1}{2}} = 0.9579$ than its value $k(gH)^{\frac{1}{2}}$ according to the long-wave theory. Thus, although the waves in question were moderately long, allowance for dispersive effects was essential to a reliable comparison with theory. As regards the magnitude of effects due to the corrugations, the experimental specifications made $\epsilon = 0.0978$, so that the number defined by (23) was 0.0266. These numbers are small enough for reasonable confidence in the approximations to first order in δ.

2.3. *Modelling of the experimental situation*

We next consider how to adapt the theory to the situation where water waves of small amplitude are observed in a channel with a corrugated bottom, with a simple-

harmonic exciter at one end and with a beach at the other. At frequencies inside the stopping band, the corrugations tend to reflect energy and so produce standing waves. Because the length of the corrugated stretch is limited, however, some energy transmission towards the beach always occurs; and so the simplest solution of the theoretical problem, describing pure (reactive) attenuation with distance from the exciter, will generally be insufficient. Outside the stopping band the rate of energy transmission will be greater, depending correspondingly more on the efficiency of the beach as an energy absorber. In all cases an adequate description requires both independent solutions of (2), or of the Stokes-wave problem treated in §2.2, which can together compose a solution satisfying an appropriate terminal condition at the beach.

The effect of the beach can reasonably be modelled as if concentrated at $x = 0$, say, and we now conveniently take x (and so also $z = kx$) to be measured positively towards the other end of the channel. In terms of the perturbed elevation ζ of the free surface, the effect of the beach is accordingly representable by the condition

$$\zeta_t - \omega\zeta_z = r(\zeta_t + \omega\zeta_z) \quad \text{at } z = 0, \tag{24}$$

in which r, the reflection coefficient, is a number satisfying $0 \leqslant r \leqslant 1$. The plausibility of (24) as a model for present purposes is supported by its obvious interpretation in the case of sinusoidal waves with any wavenumber $k = \omega/c$ in a *uniform* channel. Perfect absorption by the beach is represented by $r = 0$, for the condition $\zeta_t - \omega\zeta_z$ ($\equiv \zeta_t - c\zeta_x) = 0$ at $z = 0$ characterizes a wholly transmitted wave there; and perfect reflection is represented by $r = 1$ which makes $\zeta_z = 0$ at $z = 0$. Typically r lies between 0.1 and 0.2 for beaches in the laboratory (cf. Mahony & Pritchard 1980).

In our experiments wave amplitudes were measured as a function of distance along the channel at fixed frequencies ω. For comparison, therefore, we need predictions of the function

$$\tilde{\zeta}(z) = \tfrac{1}{2}\{\max_t \zeta(z,t) - \min_t \zeta(z,t)\}, \tag{25}$$

which is the same as $(\tilde{\zeta}_1^2 + \tilde{\zeta}_2^2)^{\frac{1}{2}}$ if $\tilde{\zeta}_1$ and $\tilde{\zeta}_2$ are the amplitudes of components of $\tilde{\zeta}$ in temporal quadrature. The prediction of ζ for wavefields in a uniform channel should first be noted. In this case a simple calculation shows (24) to imply that

$$\frac{\tilde{\zeta}(z)}{\tilde{\zeta}(0)} = \frac{(1 + r^2 + 2r\cos 2z)^{\frac{1}{2}}}{1 + r} \tag{26}$$

when viscous damping is neglected. Thus, for $r = 0$ (perfect absorption by the beach) $\tilde{\zeta}(z)$ is constant, as is obviously to be expected; and for $r = 1$ (perfect reflection) the result is $\tilde{\zeta}(z)/\tilde{\zeta}(0) = |\cos z|$, describing pure standing waves with nodes at $z = \tfrac{1}{2}\pi$, $\tfrac{3}{2}\pi, \ldots$ (i.e. $x = \tfrac{1}{4}\lambda, \tfrac{3}{4}\lambda, \ldots$). With allowance for viscous effects causing a spatial attenuation rate $\Delta k < 0$, which applies to both the incident and reflected wavetrains, the implication from (24) is that

$$\frac{\tilde{\zeta}(z)}{\tilde{\zeta}(0)} = \frac{(\mathrm{e}^{2\Delta z} + r^2\,\mathrm{e}^{-2\Delta z} + 2r\cos 2z)^{\frac{1}{2}}}{1 + r}$$

$$= \frac{\mathrm{e}^{\Delta z} + r\,\mathrm{e}^{-\Delta z}\cos 2z}{1 + r} + O(r^2). \tag{27}$$

These simple results are well known (cf. Ursell, Dean & Yu 1960; Mahony & Pritchard 1980, §5).

Proceeding to account for the effects of the bottom corrugations, we shall first use the long-wave theory in order to demonstrate the method, after which modifications required by dispersive waves can easily be recognized. The two independent solutions of (2) were originally considered in the form

$$\hat{\zeta}_{1,2}(z) = e^{\pm \mu z} \psi(\pm z),$$

where ψ is a periodic function with period 2π; and the first approximation for small δ gave

$$\psi(z) = \cos z + p \sin z,$$

in which $p = A/B$ is determined by (3), changing sign with the sign of μ. (Note that although (3) indicates $|p| \to 0$ and $|p| \to \infty$, respectively, at the lower and upper ends of the stopping band (i.e. $\beta \to 1$ and $\beta \to -1$), so that alternative explicit representations of ψ are needed in these limits, the exceptional cases will in fact be subsumed in the reduction that follows.) Suitably taking $\hat{\zeta}_1 \pm \hat{\zeta}_2$ as the independent solutions of (2) and anticipating the form of $\zeta(x, t)$ imposed by the terminal condition (24), we obtain

$$\zeta(x, t) = a(\cos z \cosh \mu z + p \sin z \sinh \mu z) \sin \omega t$$
$$+ b(\cos z \sinh \mu z + p \sin z \cosh \mu z) \cos \omega t \quad (28)$$

as an appropriate representation of the wavefield.

Substitution of (28) into (24) shows that

$$(1 - r)a = (1 + r)(p + \mu)b,$$

and the term in μ can be neglected consistently with the first approximation for small δ, provided frequency is not far from the stopping band. Hence b can be eliminated from (28), and then evaluation of (25) leads to

$$\frac{\tilde{\zeta}(z)}{\tilde{\zeta}(0)} = \tfrac{1}{2}[1 + q - p^2 - qp^{-2} + (1 + q + p^2 + qp^{-2}) \cosh 2\mu z$$
$$+ \{1 - q + p^2 - qp^{-2} + (1 - q - p^2 + qp^{-2}) \cosh 2\mu z\} \cos 2z$$
$$+ 2(p + qp^{-1}) \sinh 2\mu z \sin 2z]^{\frac{1}{2}}, \quad (29)$$

in which $q = (1 - r)^2/(1 + r)^2$. (It is noteworthy as a check that this result reduces correctly to (26) if one formally takes $\mu \to 0$, supposing p and p^{-1} to remain bounded in the limit. As will be appreciated presently, however, a more exacting account of the limit is needed for the correct interpretation of behaviour at the end-points of the stopping band.)

As a first approximation for small δ, the expression (29) can now be recognized to follow also from the dispersive-wave theory of §2.2. This correspondence becomes clear upon noting how ζ is related to the velocity potential ϕ by the boundary conditions preceding (11), noting also that the differences between (x, y) and (ξ, η) are $O(\delta)$. In the new presentation of (29) the only modifications are that μ is to be evaluated from (21) or (22) rather than (7), and that now approximately $p = C/D$, where C and D are the constants introduced in (15). Thus p is determined by either of (17), which can be simplified consistently with the first approximation for small ϵ and small $|1 - \gamma^2|$. To sum up the approximate result for dispersive waves, we have (29) with the following revised specifications: (i) μ is given by (22), in which from (20) modifying (6)

$$\beta = \frac{1 - \gamma^2}{\tfrac{1}{2}\epsilon} \qquad \left(\gamma = \frac{\omega}{\omega_0} > 0\right);$$

and (ii) by reduction from (17) and (22)

$$p = -\frac{(\frac{1}{2}\epsilon - 1 + \gamma^2)}{\mu(1+R)} = -\left(\frac{1-\beta}{1+\beta}\right)^{\frac{1}{2}}. \tag{30}$$

This result shows that, at frequencies within the stopping band ($-1 < \beta < 1$ and so $\mu > 0$), both the non-oscillatory component of $\tilde{\zeta}(z)$ and the amplitude of its oscillations increase exponentially with distance $z = kx$ from the beach. As will be exemplified in §4, experimental estimates of μ can be made by comparing measured graphs of $\tilde{\zeta}(z)$ with the prediction (29), in which an appropriate value of q is taken. It will be confirmed presently, moreover, that (29) also correctly predicts observable behaviour at the ends of the stopping band ($\beta = \pm 1$) and moderately far outside it ($\beta^2 > 1$).

2.4. *Points of interpretation*

We note several interesting aspects of the general result (29).

2.4.1. *An invariant property*

The local wave amplitude is shown by (29) to have the form

$$\tilde{\zeta} = [U + V \cos 2z + W \sin 2z]^{\frac{1}{2}},$$

in which U, V and W are smooth functions of μz, being thus slowly varying in comparison with $\cos 2z$ and $\sin 2z$. It follows that the peaks and troughs in $\tilde{\zeta}(z)$ describe envelopes given very nearly by

$$\tilde{\zeta}_{\mathrm{M}}, \tilde{\zeta}_{\mathrm{m}} = [U \pm (V^2 + W^2)^{\frac{1}{2}}]^{\frac{1}{2}}. \tag{31}$$

The slowly varying functions $\tilde{\zeta}_{\mathrm{M}}$ and $\tilde{\zeta}_{\mathrm{m}}$ are illustrated in figure 3. The definitions (31) imply that

$$\tilde{\zeta}_{\mathrm{M}} \tilde{\zeta}_{\mathrm{m}} = [U^2 - V^2 - W^2]^{\frac{1}{2}};$$

and when this expression is evaluated for U, V, W as specified in (29), it appears upon reduction that

$$\frac{\tilde{\zeta}_{\mathrm{M}} \tilde{\zeta}_{\mathrm{m}}}{\tilde{\zeta}^2(0)} = q^{\frac{1}{2}} = \frac{1-r}{1+r} \tag{32}$$

in all cases, irrespective of the values of ϵ and β and hence μ. The simple property (32) is at first sight surprising in view of the complexity of (29); but further investigation, which we pass over, shows it to represent the necessary constancy of energy transmission through the wavefield in all cases.

2.4.2. *Frequency at centre of stopping band*

When $\omega = \omega_0$ we have $\beta = 0$ and so $p = -1$ by (30). In this case μ takes its (approximate) maximum value $\frac{1}{2}\epsilon/(1+R)$ according to (22), and (29) reduces to

$$\frac{\tilde{\zeta}(z)}{\tilde{\zeta}(0)} = (1+Q)^{-\frac{1}{2}} [\cosh 2\mu z + Q \cos 2z - \sinh 2\mu z \sin 2z]^{\frac{1}{2}}, \tag{33}$$

where

$$Q = \frac{1-q}{1+q} = \frac{2r}{1+r^2}, \quad (1+Q)^{-\frac{1}{2}} = \frac{(1+r^2)^{\frac{1}{2}}}{1+r}.$$
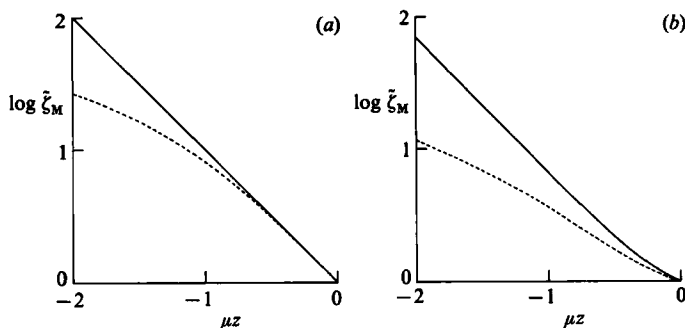
FIGURE 3. Comparisons between standing-wave envelopes $\tilde{\zeta}_M$ (cf. (31)) at the centre of the stopping band (——, $\beta = 0$) and at the low-frequency end of the stopping band (————, $\beta = 1$): (a) $r = 0$; (b) $r = 0.2$.

With $r = 0$, for example, (32) gives

$$\tilde{\zeta}_M, \tilde{\zeta}_m = \tilde{\zeta}(0) \, e^{\pm \mu z},$$

which compares with the result $\tilde{\zeta}_M = \tilde{\zeta}_m = \tilde{\zeta}(0) \exp(\Delta z)$ according to (27), for waves subject to viscous damping in a uniform channel.

2.4.3. *The case $\mu = 0$*

Taking the limits $\beta \to 1$ and $\beta \to -1$ in (29), one obtains respectively.

$$\frac{\tilde{\zeta}(z)}{\tilde{\zeta}(0)} = 2^{-\frac{1}{2}}[1 + q + q\epsilon'^2 z^2 + (1 - q + q\epsilon'^2 z^2) \cos 2z - 2q\epsilon' z \sin 2z]^{\frac{1}{2}}, \qquad (34)$$

$$\frac{\tilde{\zeta}(z)}{\tilde{\zeta}(0)} = 2^{-\frac{1}{2}}[1 + q + \epsilon'^2 z^2 + (1 - q - \epsilon'^2 z^2) \cos 2z - 2\epsilon' z \sin 2z]^{\frac{1}{2}}, \qquad (35)$$

where $\epsilon' = \epsilon/(1 + R)$. It is thus shown that prominent effects of the corrugations remain at the low-frequency end ($\beta = 1$) and high-frequency end ($\beta = -1$) of the stopping band, although $\mu = 0$ there. The wavefield can still suffer considerable attenuation along the channel towards the beach. In fact, for small r and for a moderate total length of the channel ($\epsilon' z$ limited to about 5, say), the envelope functions $\tilde{\zeta}_M$ and $\tilde{\zeta}_m$ corresponding to either (34) or (35) turn out not to differ greatly from those corresponding to (33) at the centre of the stopping band. The formula (29) consequently needs to be applied with considerable precision in estimating μ from experimental observations in a channel of moderate length.

The results (34) and (35) reflect the fact that for $\mu = 0$ the original problem has a periodic solution, but there is a second, non-periodic solution which is also needed to satisfy the terminal condition at the beach. For example, in the case $\beta = 1$, the two solutions of (2) approximated to $O(\delta)$ are

$$\hat{\zeta}_1 = \cos z - \tfrac{3}{16}\delta \cos 3z, \quad \hat{\zeta}_2 = \sin z - \delta(\tfrac{1}{2}z \cos z + \tfrac{3}{16} \sin 3z).$$

Rederiving the dispersive-wave theory *ab initio* in each of the special cases $\beta = \pm 1$, one has to consider one periodic and a second non-periodic form for the potential ϕ in place of (15); but the outcome merely confirms the approximations (34) and (35).

2.4.4. *The case $\beta^2 > 1$*

For frequencies outside the stopping band, we may write $\mu = i\nu$, where according to (22) the real number ν is given by

$$\nu = \frac{\frac{1}{2}\epsilon(\beta^2 - 1)^{\frac{1}{2}}}{1 + R} > 0. \tag{36}$$

The formula (29) still gives $\tilde{\zeta}$ as a positive real function, becoming upon rearrangement

$$\frac{\tilde{\zeta}(z)}{\tilde{\zeta}(0)} = [(\beta^2 - 1)(1 + Q)]^{-\frac{1}{2}}[\beta^2 - \beta Q + (\beta Q - 1)\cos 2\nu z$$
$$+ \{\beta - Q + \beta(\beta Q - 1)\cos 2\nu z\}\cos 2z + (\beta Q - 1)(\beta^2 - 1)^{\frac{1}{2}}\sin 2\nu z \sin 2z]^{\frac{1}{2}}. \tag{37}$$

Here Q is as defined below (33). The approximations underlying the formula (37) limit its applicability in the present case to ranges of frequency above and below but comparable in width with the stopping band, such that ν remains a small fraction. The main feature revealed, to which our experimental observations were directed, is that the wavefield has gradual sinusoidal modulations with period π/ν in z, so $\pi/\nu k$ in x.

For an experimental channel in which the stretch with a corrugated bottom has length D, say, it is clear that this new feature will not be prominent unless $|1 - \gamma^2|$ is made significantly larger, by a margin depending inversely on D, than its value at the ends of the stopping band. That is, the anticipated oscillations in the envelopes $\tilde{\zeta}_M$ and $\tilde{\zeta}_m$ may not be discernable until at least one period $\pi/\nu k$ is covered in the available length D. In general, observations at frequencies only marginally outside the stopping band are difficult to interpret, and $|\beta|$ needs to be raised well above 1 (to about 2 in our experiments) before measurements of ν become feasible in the simple way suggested.

The number Q is positive unless the beach is perfectly absorbing. Therefore, because of the factor $\beta Q - 1$ common to the terms in (37) that describe the gradual modulations, the effects represented are, for the same $|\beta|$, more prominent on the high-frequency side ($\beta < -1$) than on the low-frequency side ($\beta > 1$). A curious indication by (37) is that for $\beta = 1/Q$ the modulations disappear, leaving $\tilde{\zeta}$ featureless except for uniform oscillations with the wavelength of the bottom corrugations. As Q is usually quite small, however, this critical value of β may be too high for the present approximations to be reliable.

Finally, note the following simple check on (37). Take the formal limits $\beta \to -\infty$ and $\beta \to \infty$ with ν held fixed, so that $\epsilon \to 0$ since $\frac{1}{2}\epsilon|\beta|/(1 + R) \to \nu$ according to (36). The results are

$$\frac{\tilde{\zeta}(z)}{\tilde{\zeta}(0)} = (1 + Q)^{-\frac{1}{2}}[1 + Q\cos 2(1 \pm \nu)z]^{\frac{1}{2}}, \tag{38}$$

which recover (26) representing uniform wavefields with basic wavenumbers $(1 \pm \nu)k$. Because $\frac{1}{2}\beta\epsilon = 1 - \gamma^2 = (\omega_0^2 - \omega^2)/\omega_0^2$ by the original definition of β, it follows that to first order in $|\omega - \omega_0|/\omega_0$ these wavenumbers are both given by

$$k\left\{1 + \frac{2}{(1 + R)}\frac{(\omega - \omega_0)}{\omega_0}\right\}.$$

This result is precisely as must be expected, since $\frac{1}{2}(1 + R)(\omega_0/k)$ is the group velocity $d\omega/dk$ of Stokes waves at the frequency ω_0.

3. Experiments

3.1. *Apparatus*

The experiments were made in a glass-sided channel of span 0.30 m and length 6 m. The bed of the channel was carefully levelled, so that its deviation from a mean horizontal plane was reduced to less than 0.4 mm, and the width of the channel was uniform to within 0.2 mm. A false bottom, composed of a layer of expanded polystyrene into which sinusoidal corrugations had been cut, was wedged into the channel, seated on the original bed. A wavemaker was placed near one end of the channel, and a rigid plane beach with slope 1 in 10 was fixed at the other end.

The wavemaker consisted of a plate suspended on a horizontal shaft, whose axis was normal to the walls of the channel at a height of about 1 m above the bed. The gaps between the edges of the plate and the sides and bed of the channel were packed with foam plastic to restrict leakage past the wavemaker. The plate was driven in an oscillatory motion by a long crank keyed to an eccentric on the shaft of a stepping motor. The constant-frequency signal operating the motor was derived by countdown from a crystal oscillator, the stability of which ensured extremely precise control of the wavemaker.

The false bed of the tank was arranged in the following way. The first 0.94 m was a horizontal plane surface at the mean height of the corrugations that lay beyond this flat section. The corrugations, with wavelength 0.18 m and amplitude 3.5 mm, extended a further 4.32 m along the channel and were terminated by a smooth join to the beach. There was a total of 23 crests in the corrugated section.

To make the corrugated section we cut two templates to the desired profile of the bed and fixed these on either side of a block of polystyrene. A heated wire stretched straight perpendicularly to the templates was then dragged through the polystyrene, its movement being guided by the templates. By careful adjustments to the temperature of the wire and the speed at which it was pulled, an accurate clean cut could be made in the polystyrene. After the bed had been wedged into the tank, the uniformity of the corrugated section was checked by measurements of the depth of the crests below the surface of still water. These measurements, both across and along the channel, showed that the vertical locations of the crests varied more or less randomly about their mean level with a standard deviation of about 0.6 mm.

The heights of waves on the water surface were measured by means of small proximity transducers placed just above the surface (cf. Barnard & Pritchard 1972). The output from the transducers was relayed to an ultraviolet chart recorder, giving a continuous record of the surface elevation. Wave amplitudes in the present experiments were typically 0.1–0.2 mm and were measured with an accuracy of about 2 or 3%.

Except for the false bed, this basic apparatus was the same as used by Buchan (1979), by Mahony & Pritchard (1980) and by Bona, Pritchard & Scott (1981), whose accounts include further details of the equipment and experimental methods.

3.2. *Experimental procedure*

The tank was filled with water to roughly the desired depth and surface films were skimmed off. The water was then topped up until the level was within 0.01 mm of a reference level, set by the tip of a pointer gauge. For all the experiments to be described here, the mean depth of water was nominally 30 mm. Due to the residual variability of the corrugations as already noted, however, the actual mean depth was not known with the same high accuracy as the adjustments to the reference level.

(We also made measurements using a corrugated bed with wavelength 0.15 m and amplitude 4.5 mm in water of depth 37.5 mm. The results of these other experiments were found to be consistent with those reported here.)

When the required water level had been established, the wavemaker was started oscillating at the desired frequency and measurements of the local waveform were taken at 30 mm intervals along the working section of the channel. These records were then used to determine the distance-dependent wave amplitude, namely the real function $\tilde{\zeta}(z)$ in the equation

$$\zeta(x,t) = \tilde{\zeta}(z)\,\sin\left[\omega t + \theta(z)\right]$$

describing the vertical displacement of the free surface (cf. (25)). Here $z = kx = 2\pi x/\lambda$ and θ is a phase number which generally varies with z but does not need evaluation in the present investigation.

4. Experimental results

The main specifications of the experiments are listed underneath table 1, which presents various experimental results to be explained below. The quantity Λ, called the basic wavelength, is the wavelength of waves with radian frequency $\omega = 2\pi/T$ in a uniform channel of depth H; it is given implicitly by the dispersion relation

$$\omega^2 = \frac{2\pi g}{\Lambda}\tanh\left(\frac{2\pi H}{\Lambda}\right). \tag{39}$$

As indicated in the table, the values of T were chosen so that Λ was increased in steps of 10 mm. For the conditions of these experiments, the periods T_c corresponding to the critical values γ_c of γ that mark the ends of the stopping band are 0.6763 and 0.7103 s. It is thus seen that the periods prescribed in the experiments extended well beyond the theoretical extremities of the stopping band. The fact that the period for experiment (f) coincided to four decimal places with that at one end of the stopping band was coincidental.

4.1. *Main features of results*

The primary experimental results are recorded in figure 4, where $\tilde{\zeta}/H$ is plotted as a function of z ($= kx$), with the origin for z taken at the wavemaker and with z increasing towards the beach. An obvious adjustment is needed and no confusion should arise regarding our previous use of z, in (24) *et seq.*, to denote distance from the beach towards the wavemaker. The interruption of the records near $z = 44$ is due to an obstruction above the tank which impeded measurements. The straight vertical lines near $z = 19$ indicate the start of the corrugated section, and the positions of the crests of the corrugations are also marked. It is worth noting that each of the component graphs in figure 4 presents nearly 160 separate measurements taking many hours to collect.

The classes of behaviour described in §§2.3 and 2.4 are evident from these graphs. The wave amplitude $\tilde{\zeta}(z)$ is seen to have an oscillatory component with roughly the same wavelength as the corrugations on the channel bed; it is nearly uniform above the initial flat section of the channel but is modulated over the subsequent corrugated section. In figure 4(a–c), at periods well below the critical value $T_c = 0.6763$, the modulations are seen to be regularly oscillatory in z (cf. (37)), with a wavelength that increases as T approaches T_c. Estimates of the wavelength L of

Expt	Basic wavelength Λ (mm)	Period T (s)	$\gamma^2 = (0.6927/T)^2$	Viscous decay length L_v (m)	Envelope wavelength L (m)	μ	Carrier wavelength l (mm)
a	320	0.6223	1.239	9.44	2.76	0.130i	163
b	330	0.6399	1.172	8.33	4.02	0.0895i	169
c	340	0.6574	1.110	—	6.04	0.0597i	175
d	350	0.6751	1.053	—	—	0†	179
e	360	0.6927	1.000	—	—	0.0290	180
f	370	0.7103	0.951	—	—	0.0058	180
g	380	0.7282	0.905	—	10.10	0.0355i	184
h	390	0.7461	0.862	9.36	5.12	0.0704i	189
i	400	0.7637	0.823	11.59	3.72	0.0968i	192

† cf. §4

CONSTANTS: $H = 30.0$ mm; $\tfrac{1}{2}\lambda = 180$ mm ($k = 0.0175$ mm^{-1}); $\delta = 0.117$; $\epsilon = 0.0978$ (cf. (14)); $\gamma_c^2 = 1.0489, 0.9511$ (cf. (19)).

TABLE 1. Summary of the experimental data. The quantities Λ, L_v, L, μ and l are defined in the text of §4.
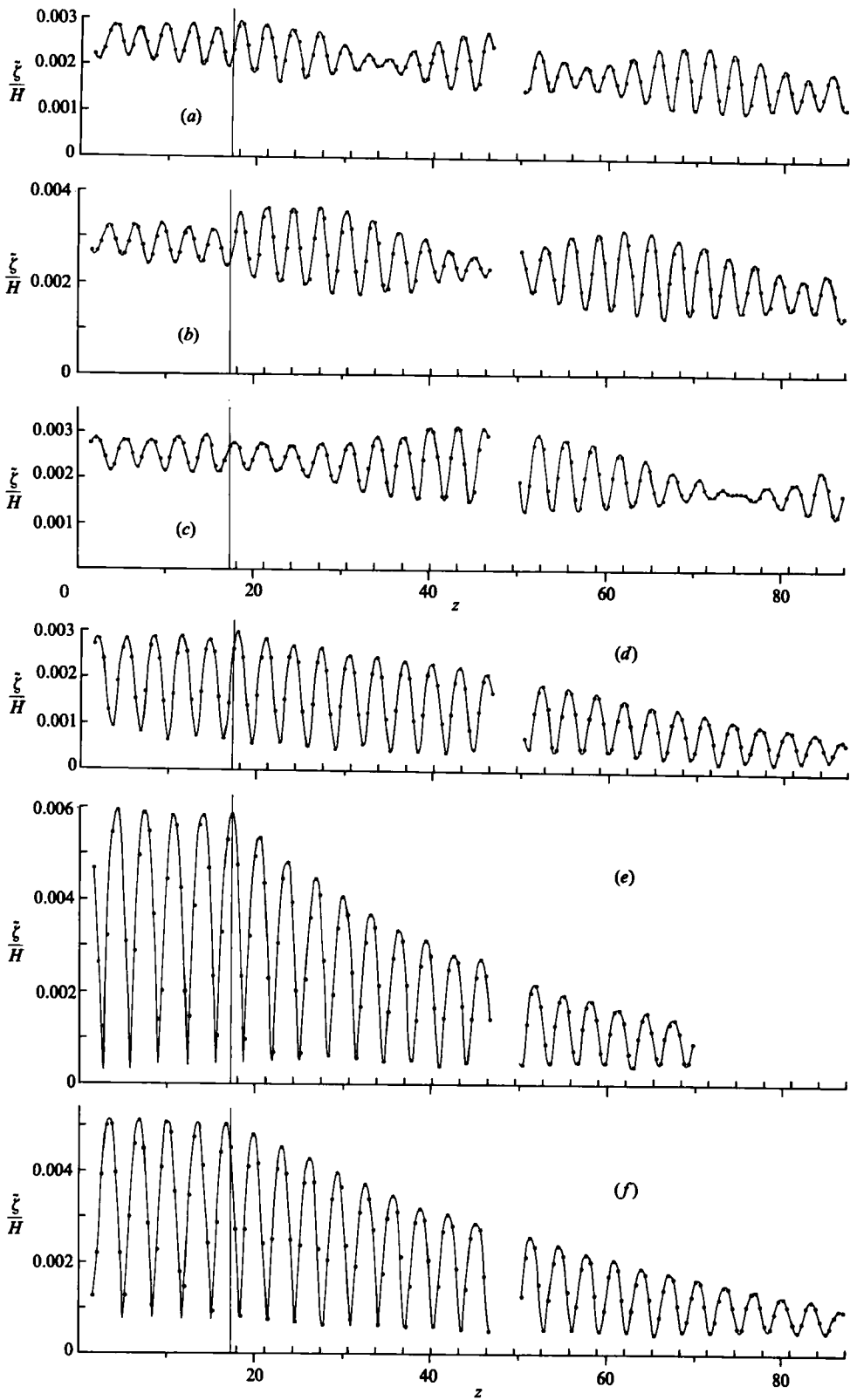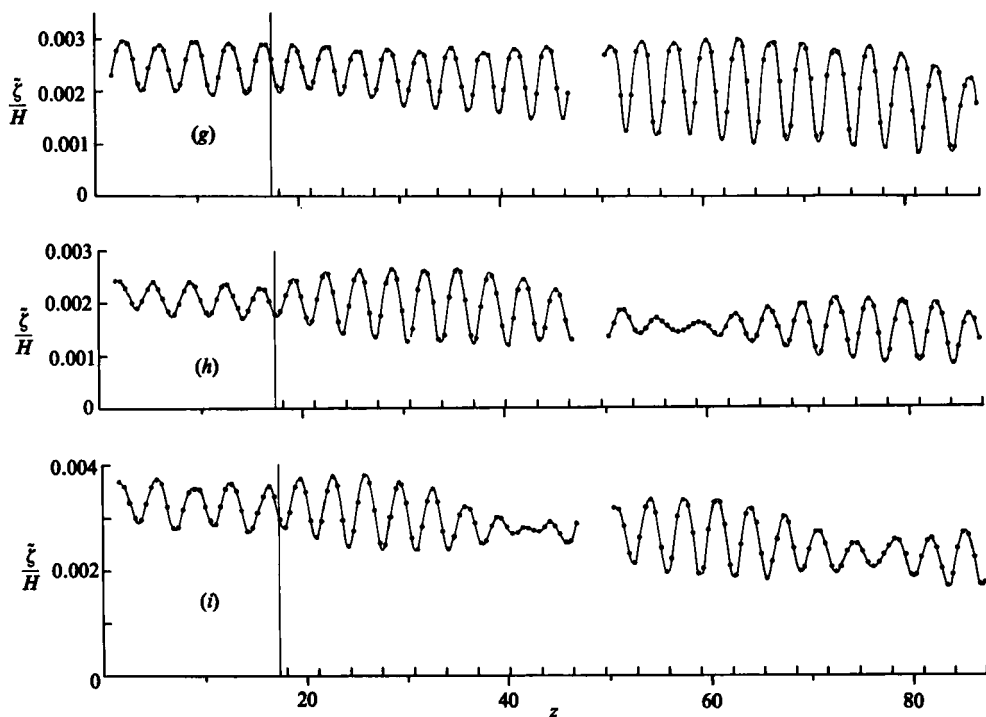
FIGURE 4(*a–f*). For caption see facing page.

FIGURE 4. Measured wave amplitudes $\tilde{\zeta}/H$ as a function of distance z along the channel. (a) $T = 0.6223$ s; (b) 0.6399 s; (c) 0.6574 s; (d) 0.6751 s; (e) 0.6927 s; (f) 0.7103 s; (g) 0.7282 s; (h) 0.7461 s; (i) 0.7637 s.

these modulations are included in the fifth column of table 1. Similar estimates were also made for experiments (g), (h) and (i), but not for experiments (d), (e) and (f) which were at periods T either too close to or within the stopping band. The wavelengths l attributable to the fast oscillations of $\tilde{\zeta}(z)$ have also been determined from these graphs and are given in the last column of table 1. (Comparisons of these estimates for L and l with the theoretical predictions of §2 will be made below.)

Another feature evident in figure 4 for experiments (a), (b), (c) and (g), (h), (i) is the gradual reduction, with distance along the channel, undergone by the local mean value of $\tilde{\zeta}/H$. This feature arises from the attenuation of outward-travelling waves, as indicated in (27), through viscous damping at the bed and sidewalls of the channel together with possible damping effects at the free surface. On the assumption that outward-travelling waves decay according to $\exp(-x/L_v)$ (cf. (27)), estimates of the dissipative length-scale L_v have been made from the data for experiments (a), (b), (h) and (i), and the results are included in table 1. It is plain that, although not insignificant, dissipative effects were a secondary feature of the experiments and in no case dominated the effects principally in question. The mean value L_v of the estimates for L_v quoted in table 1 is 9.68 m, and thus $(kL_v)^{-1} = 5.92 \times 10^{-3}$, which number will be used later in making corrections for dissipative effects.

The results of experiments (d), (e) and (f), carried out at periods very near to or within the stopping band, exemplify the behaviour anticipated in §2.3 (see (29) and (33)). For example, the local maxima in $\tilde{\zeta}$ are seen, as expected, to decay more or less exponentially with z.
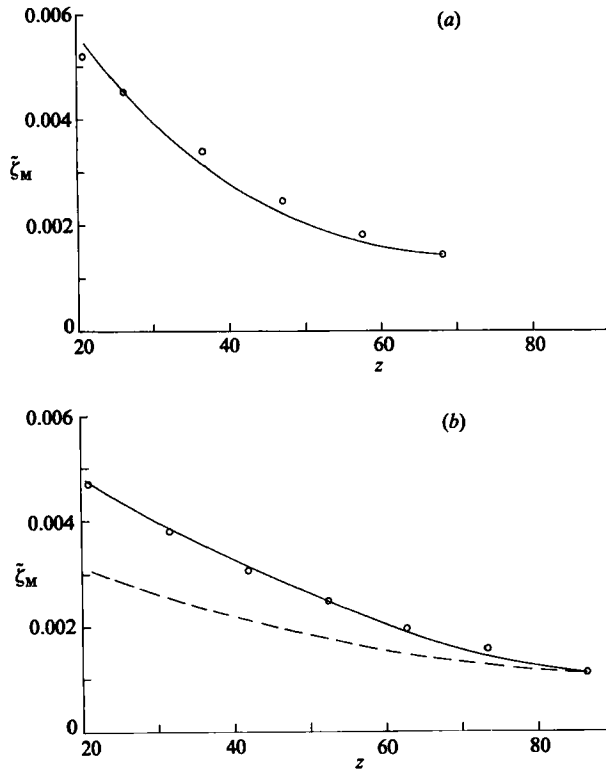
FIGURE 5. Comparisons between measurements of wave envelopes $\tilde{\zeta}_M$ and theoretical curves for $\tilde{\zeta}_M(z)$. (a) Experiment (e) at $T = 0.6927$ s; —— based on (29). (b) Experiment (f) at $T = 0.7103$ s; —— based on (29); ---- based on (34).

4.2. Comparisons with theory

We shall now make various quantitative comparisons between the observations and the theoretical results described in §2. First consider experiment (e) for which the period $T = 0.6927$ s, near the centre of the stopping band. Let us suppose that the observed local maxima $\tilde{\zeta}_M^*$ of $\tilde{\zeta}$ are well represented by (29) together with (31), but the decay rate μ is a free parameter. Thus an empirical estimate for μ can be obtained by determining the value of μ that minimizes the difference between $\tilde{\zeta}_M$ as given by (29) and $\tilde{\zeta}_M^*$ as determined experimentally. Representative values of $\tilde{\zeta}_M^*$ at positions z_i, $i = 1, ..., N$, were obtained from the data, and the value of μ was determined giving a global minimum of the quantity

$$F(\mu) = \sum_{i=1}^{N} \{\tilde{\zeta}_M^*(z_i) - \tilde{\zeta}_M(\mu, z_i)\}^2. \tag{40}$$

In order to specify $\tilde{\zeta}_M$, however, an appropriate value for the amplitude of the reflected wave at the far end of the channel is needed to fix q. For experiment (e) measurements of $\tilde{\zeta}$ were obtained only as far as $z = 70$. Let us proceed, therefore, by specifying r from the measurements of $\tilde{\zeta}(z)$ near $z = 70$; that is, take

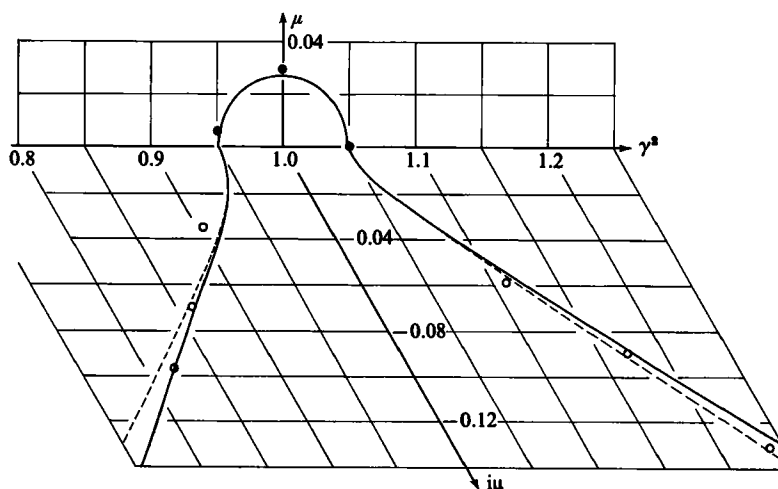$$r = \frac{\tilde{\zeta}_M - \tilde{\zeta}_m}{\tilde{\zeta}_M + \tilde{\zeta}_m}, \tag{41}$$

FIGURE 6. Comparison between empirically determined values of μ and the theoretical predictions (19) (——) and (21) (----). The points ● were determined from decay rates, and ○ from the wavelengths of the envelopes of $\tilde{\zeta}(z)$ shown in figure 4.

where $\tilde{\zeta}_M$ and $\tilde{\zeta}_m$ are respectively the local maximum and minimum of $\tilde{\zeta}$ near $z = 70$, and use this estimate of r to evaluate q in (29). For experiment (e) this procedure assigns r a value approximately 0.595, for which the corresponding value of q is 0.0655. The value of μ hence found to minimize F is $\mu = 0.03495$. (The minimum is quite sharp for, in contrast with the (normalized) value $F = 1.0$ at $\mu = 0.03495$, it is found that $F = 5.2$ with $\mu = 0.034$ and $F = 1.6$ with $\mu = 0.036$.) A comparison between the empirical values of $\tilde{\zeta}_M^*(z)$ and the function $\tilde{\zeta}_M(z;\mu)$, with this optimal value of μ, is shown in figure 5(a). (Note that, by assuming the channel to terminate near $z = 70$ in order to make an estimate for r, we imply the slope of $\tilde{\zeta}_M$ to be zero there and so incapable of matching that of $\tilde{\zeta}_M^*$ exactly.)

Now the total decay rate of $\tilde{\zeta}$ is a combination of that due to the blocking effect of the corrugations and that due to the dissipative effects noted above. Since the dissipation evidently had a minor role in these experiments, let us suppose that the observed decay rate of $\tilde{\zeta}_M$ is the linear sum of the two effects. It then follows that an empirical estimate for the blocking effect of the corrugated bed is that the decay coefficient $\mu = 0.0350 - (kL_v)^{-1} = 0.0290$, which number coincides with the theoretically estimated value of μ quoted in table 1. This value of μ is plotted in figure 6, where the theoretical distribution for $\mu(\gamma^2)$, determined from (18), is also given. (The dashed curve shown in figure 6 is the approximate form (21) for μ.)

[Note that the value of r used in the above calculations does not correspond to the reflection coefficient at the beach at the far end of the channel. Rather it is an empirical estimate of the relative amplitudes of the forward and backward-travelling waves near $z = 70$. An estimate of the reflection coefficient of the beach is probably most easily made from experiments (a) and (i), which indicate a value of about 0.14. This value for r accords with those reported by Mahony & Pritchard (1980). It is easy to verify that the formula (41) for r, with $\tilde{\zeta}_M$ and $\tilde{\zeta}_m$ defined by (31) in terms of $\tilde{\zeta}$ defined by (25), is equivalent to the formula (24) as originally referred to the beach. While various other representations are possible, (41) is best suited to empirical estimates of the local reflection coefficient that varies along the tank. As expressed

estimates of the local reflection coefficient that varies along the tank. As expressed most usefully by (41), r is essentially the same as the reflection coefficient otherwise represented and denoted K_R by Davies & Heathershaw (1984), R by Mei (1985) and Kirby (1986a, b).]

Similar comparisons have been made with the results of experiments (d) and (f). Experiment (f) deserves special attention since the chosen period $T = 0.7103$ s happened to equal the theoretical value T_c corresponding to the low-frequency end of the stopping band. Thus the formula (34) for the limiting case $\beta = 1$ might be expected to apply. At the right extremity of the records in figure 4 (f), specifically at $z = 87$, it is estimated that $r = 0.363$ and so $q = 0.218$. Hence, when amplified by an exponential factor with exponent kL_v to allow for dissipative effects, the formula (34) gives the dashed curve for ζ_M included in figure 5(b). This curve can be seen not to agree well with the experimental results; however, the discrepancy is explainable readily enough by the sensitivity of μ to small changes of T in the neighbourhood of each special value T_c. (Note that $\mu(\gamma^2)$ is not a continuously differentiable function at the ends of the stopping band (see (21) and figure 6).) Resort to the more general formula (29) is therefore warranted, and we may use the same test as applied to experiment (e). For example, let us take $T = 0.7100$ s instead of 0.7103 s for experiment (f). Then the minimum of F as defined by (40) is found to be achieved with $\mu = 0.0117$; and the substitution of this value in (29) gives the continuous curve in figure 5(b), which is in far more satisfactory agreement with the experimental results. Subtracting as before the estimated exponent that allows for dissipative effects, one obtains for μ the empirical estimate 0.0052, which is plotted in figure 6 and compares with the theoretical value 0.0047 at the frequency in question.

Experiment (d) was at $T = 0.6751$ s, just below the theoretical value $T_c = 0.6763$ s for the high-frequency end of the stopping band. Thus a small imaginary value of μ might be expected; but the estimation of μ presented uncertainties. (Their inevitability may be appreciated in the light of the fact that an error in the estimate of λ as small as 0.5 mm, or in the estimate of H about 0.1 mm, would be enough to put the operating period $T = 0.6751$ s within the stopping band.) The records in figure 4(d) suggested $r = 0.455$ and so $q = 0.141$ at $z = 87$, which value of q was used in comparisons based as before on (29) or its equivalent version (37). With $\beta = -1.080$ corresponding to $T = 0.6571$ s, our least-squares method referred to (37) led to an estimate of μ roughly $0.01i$. On the other hand, by taking instead $T = 0.6767$ s just inside the stopping band, a fairly close optimal fit with the experimental results was obtained from (29) with $\mu = 0.005$. On balance it appeared well justified to take $\mu = 0$ as the representative estimate. In fact, strongly supporting this estimate, an evaluation of the formula (35) for $\beta = -1$ was found to give a reasonably close approximation to the measured profile of $\tilde{\zeta}_M^2 - \tilde{\zeta}_m^2$, which approximation was virtually indistinguishable from the second of those described above.

With contrasting ease, at frequencies well outside the stopping band, the real number $\nu > 0$ in the representation $\mu = \pm i\nu$ can be estimated directly from the observed wavelength of the gradual modulations imposed on $\tilde{\zeta}(z)$. The relation between ν and this wavelength was explained below (37) in §2.4. The values so obtained, from the experimental runs (a), (b), (c), (g), (h) and (i), are quoted in table 1 and are plotted as open circles in figure 6. Again there is quite good agreement with the theoretical prediction derived from (29), here more suitably considered in its version (37).
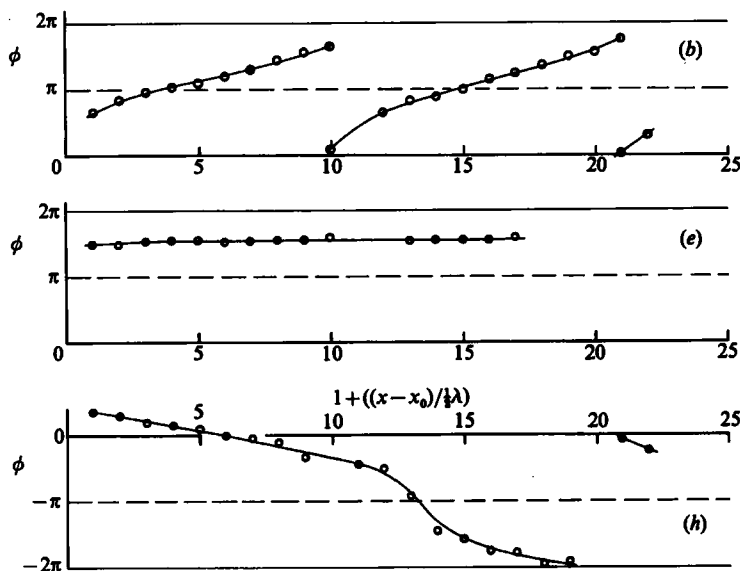
FIGURE 7. The observed phase ϕ of local minima of $\tilde{\zeta}(z)$ relative to the crests of the corrugations on the bed. Positive values of ϕ correspond to the minimum $\tilde{\zeta}$ occurring at a smaller value of z than that of the relevant crest on the bed. Here x_0 denotes the distance from the wavemaker to the crest of the first corrugation. Figure labels (b), (e) and (h) correspond to those of the experiments in table 1.

4.3. *Local properties of fast oscillations*

From the records of $\tilde{\zeta}(z)$ presented in figure 4, further comparisons with theory can be made in respect of the fast oscillations whose spacings are comparable with the wavelength $\frac{1}{2}\lambda$ of the corrugations on the channel bottom. In particular, the measured positions of local maxima and minima of $\tilde{\zeta}(z)$ relative to the corrugations illuminate differences in behaviour inside and outside the stopping band of frequencies.

Figure 7 shows a representative sample of such measurements, for the experimental runs (b), (e) and (h) at frequencies respectively above, inside and below the stopping band. For each of the three cases the estimated phase ϕ of local minima of $\tilde{\zeta}(z)$ relative to adjacent crests in the corrugations is plotted against the numbering of corrugations, so in effect against distance along the channel in units of $\frac{1}{2}\lambda$.

The theory developed in §2 shows that, at frequencies within the stopping band, the fast oscillations of $\tilde{\zeta}(z)$ should be locked in phase with the corrugations (cf. (29) with $\mu^2 > 0$). This property is confirmed convincingly by figure 7(e). It was also found to be borne out, although not quite so precisely, by corresponding estimates from the experimental runs (d) and (f) near the extremities of the stopping band. Approximate confirmation of the property in question may be seen directly by inspection of figures 4(d) and 4(f).

At frequencies outside the stopping band the fast oscillations of $\zeta(z)$ are no longer locked in phase with the corrugations (cf. (37)), and this property is exhibited plainly in figures 7(b) and 7(h). In experiment (b), for example, the phase ϕ was found to increase with distance at a more or less constant rate until a phase reversal occurred in the region near the 10th corrugation where the amplitude of the fast oscillations was smallest. Thereafter, for a new sequence of minima of $\tilde{\zeta}(z)$, the phase ϕ again increased at nearly the same rate as before. On the other hand, figure 7(h)
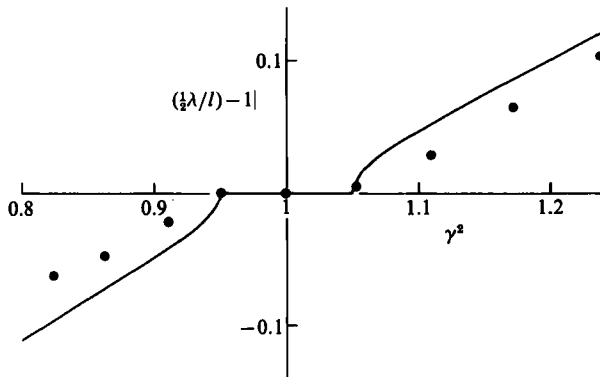
FIGURE 8. Measurements of the fractional change of local wavenumber for the fast oscillations of $\tilde{\zeta}(z)$, plotted as a function of γ^2. The curve —— describes the quantity $-\nu \operatorname{sgn}(\beta)$.

exemplifies the gradual reduction in ϕ that was observed at frequencies below the stopping band. The rate of reduction is seen to have been more or less steady in two stretches separated by the region between the 12th and 14th corrugations, where the amplitude of the fast oscillations became small and so phase estimates became unreliable.

Figure 7 illustrates the resources for finding the typical wavelength l of the fast oscillations, the estimates of which are included in table 1. Attention is restricted to regular sequences of minima of $\tilde{\zeta}(z)$ away from regions of phase reversal, and averages of the spacings are taken. Although appreciable local variations in l arose from the measurements in experiments (c), (g), (h) and (i), the estimated averages of l appear to be adequately representative.

As shown by (38), the local wavelength $2\pi l/\lambda$ of $\tilde{\zeta}(z)$ approaches $\pi(1 \pm \nu)$ as $\beta \to \pm \infty$ when ν is a fixed positive real number. In other words, we should have $(\frac{1}{2}\lambda/l) - 1 \approx \pm \kappa$ at frequencies respectively well above and well below the stopping band. In figure 8 our experimental values of $(\frac{1}{2}\lambda/l) - 1$ are accordingly compared with ν computed from (29) or (37), being plotted as a function of γ^2. The main features of the function $\nu(\gamma^2)$ are seen to be duplicated by the measurements of $(\frac{1}{2}\lambda/l) - 1$; in particular, the observed property of phase-locking within the stopping band is re-emphasized in the figure. The fact that the experimental values of $(\frac{1}{2}\lambda/l) - 1$ and the computed ν are notably separate a little way above and below the stopping band is understandable, not particularly because of experimental error but rather because the definition of l is inherently tenuous in these ranges γ^2.

5. Conclusion

As presented in §§4.2 and 4.3, the various quantitative checks on the experimental results support confidence in the reliability of the theory developed in §2. In particular, the comparisons illustrated in figure 6 and the observations of phase-locking only within the stopping band of frequencies are convincingly confirmative. The limitations of the theory should be re-acknowledged, namely its assumption of small enough wave amplitudes for nonlinear effects to be negligible and also its assumption that the amplitude of the corrugations is a reasonably small fraction $(\delta \ll 1)$ of the mean water depth H. Even though confined to small-amplitude waves, the present experiments nevertheless serve to exemplify the high level of precision

needed for a satisfactorily explicable record of the wavefield over a corrugated bed.

Let us finally return to the ideas about sand-bar formation mentioned near the beginning of §1. They deserve a little more commentary as motivation for this investigation and for related experimental work yet to be reported; but it has to be admitted that our views regarding the relevance of all such findings to oceanographic events remain extremely cautious. The variety and complexity of field observations, such as the few cited at the start in §1, underscore reasons for caution.

From laboratory tests such as providing figure 1 it was evident to us that, even when the incident surface waves are at the same frequency over long times, the evolution of a sand beach under wave action commonly depends on several different processes which may interact with and succeed each other in largely inextricable fashion. Among these contributory processes the induction of standing waves by Bragg reflection, as examined in the present paper, is likely to be a comparatively minor although not necessarily insignificant one. On the other hand, the main redistribution of sand on a beach seems most often to occur in regions where locally intense eddying motion of the water lift significant quantities of sand, which regions may be associated with wave breaking (cf. Lau & Travis, 1973, p. 4489). In our other experiments represented here by figure 1, there usually were short periods (e.g. 15–30 min) during which the beach profile underwent major changes, and they were followed by comparatively long intervals (e.g. 25–30 h) during which only small changes in the beach profile accumulated. Occasionally, during an interval of relative quiescence, when conditions happened to be right, it appeared that a slowly cumulative process entailing quasi-resonant reflection was probably operative. For we noticed in these particular experiments over many hours that a standing-wave component of the motion gradually grew, eventually breaking and generating large turbulent zones, whereupon there began a period of relatively fast change in the beach profile. Such observations have reinforced our belief that the present results may have some bearing on coastal sand-bar formation, albeit perhaps only in special instances; but fuller discussion of these other observations has to be left as a separate story.

REFERENCES

BARNARD, B. J. S. & PRITCHARD, W. G. 1972 Cross waves. Part 2. Experiments. *J Fluid Mech.* **55**, 245–256.

BONA, J. L., PRITCHARD, W. G. & SCOTT, L. R. 1981 A comparison of laboratory experiments with a model equation for water waves. *Phil. Trans. R. Soc. Lond.* A **302**, 457–510.

BRILLOUIN, N. 1953 *Wave propagation in periodic structures*. Dover.

BUCHAN, S. 1979 Edge waves on plane beaches. M.Sc. dissertation, University of Essex.

DAVIES, A. G. & HEATHERSHAW, A. D. 1984 Surface-wave propagation over sinusoidally varying topography. *J. Fluid Mech.* **144**, 419–443.

ELACHI, C. 1976 Waves in active and passive periodic structures: a review. *Proc. IEEE* **64**, 1666–1698.

KIRBY, J. T. 1986*a* A general wave equation for waves over rippled beds. *J. Fluid Mech.* **162**, 171–186.

KIRBY, J. T. 1986*b* On the gradual reflection of weakly nonlinear Stokes waves in regions with varying topography. *J. Fluid Mech.* **162**, 187–209.

LAU, J. & TRAVIS, B. 1973 Slowly varying Stokes waves and submarine longshore bars. *J. Geophys. Res.* **78**, 4489–4497.

MAHONY, J. J. & PRITCHARD, W. G. 1980 Wave reflexion from beaches. *J. Fluid Mech.* **101**, 809–832.

MEI, C. C. 1985 Resonant reflection of surface waves by periodic sandbars. *J. Fluid Mech.* **152**, 315–335.

MITRA, A. & GREENBERG, M. D. 1984 Slow interactions of gravity waves and a corrugated bed. *Trans. ASME* E: *J. Appl. Mech.* **51**, 251–255.

RHINES, P. 1970 Wave propagation in a periodic medium with application to the ocean. *Rev. Geophysics Space Phys.* **8**, 303–319.

SAYLOR, J. H. & HANDS, E. B. 1970 Properties of longshore bars in the Great Lakes. *Proc. XII Conf. Coastal Engng* vol. 2, pp. 839–853.

SHORT, A. D. 1975 Multiple offshore bars and standing waves. *J. Geophys. Res.* **80**, 3838–3840.

STOKER, J. J. 1957 *Water waves.* Interscience.

URSELL, F., DEAN, R. G. & YU, Y. S. 1960 Forced small-amplitude water waves; a comparison of theory and experiment. *J. Fluid Mech.* **7**, 33–52.